10.1002/anie.201908357

Bioinspired Core-Shell Nanoparticles for Hydrophobic Drug Delivery

Guangze Yang,[a] Yun Liu,[a] Haofei Wang,[a] Russell Wilson,[a] Yue Hui,[a] Lei Yu,[a] David Wibowo,[a] Cheng Zhang,[a,b] Andrew K. Whittaker,[a,b] Anton P. J. Middelberg,[a,c] and Chun-Xia Zhao*[a]

[a] G. Yang, Y. Liu, H. Wang, R. Wilson, Dr. Y. Hui, Dr. D. Wibowo, Dr. C. Zhang, Prof. Dr. A. Whittaker, Prof. Dr. A. P. J. Middelberg, A/Prof. Dr. C. Zhao
Australian Institute for Bioengineering and Nanotechnology
The University of Queensland
St. Lucia, Queensland 4072 (Australia)
E-mail: z.chunxia@uq.edu.au

[b] Dr. C. Zhang, Prof. Dr. A. Whittaker
ARC Centre of Excellence in Convergent Bio-Nano Science and Technology
The University of Queensland
St. Lucia, Queensland 4072 (Australia)

[c] Prof. Dr. A. P. J. Middelberg
Faculty of Engineering, Computer and Mathematical Sciences
The University of Adelaide
Adelaide, South Australia 5005 (Australia)

Abstract: With 40% of approved drugs and 90% of drugs in the pipeline being insoluble in water, developing methods to formulate and deliver hydrophobic drugs becomes urgent but remains a challenge. A large range of nanoparticles have been developed to encapsulate hydrophobic drugs. However, drug loading is usually less than 10% or even 1%. Herein, we report the fabrication of core-shell nanoparticles having exceptionally high drug loading up to 65% (drug weight/the total weight of drug-loaded nanoparticles) and high encapsulation efficiencies (>99%) based on modular biomolecule templating. Bifunctional amphiphilic peptides are designed to not only stabilize hydrophobic drug nanoparticles but also induce biosilicification at the nanodrug particle surface thus forming drug-core silica-shell nanocomposites. This platform technology is highly versatile for encapsulating various hydrophobic cargos. Furthermore, the high drug loading nanoparticles lead to better in vitro cytotoxic effects and in vivo suppression of tumor growth, highlighting the significance of using high drug loading nanoparticles.

Introduction

Over the past decades, a plethora of approaches have been developed to formulate poorly soluble drugs for improved bioavailability, safety, and efficacy.[1] With about 40% of approved drugs and 90% of drugs in the pipeline exhibiting poor water solubility, there is tremendous interest to develop new systems to deliver hydrophobic drugs.[2] Various nanoparticles have been designed for drug delivery with therapeutics either loaded inside the particles or conjugated to the particle surface.[3] However, one of the major challenges hindering their practical applications is the low drug loading (the mass fraction of drug in the entire drug-loaded nanoparticle, w/w). For the various nanoparticle systems reported, drug loading is usually below 10%.[2b, 4] For example, polymeric nanoparticles often have a drug loading lower than 5% or even less than 1%.[4d-f] Clearly, there is an urgent need to develop nanoparticles with high drug loading.

Only a small number of studies attempted to improve drug loading.[5] To inhibit drug molecule packing and subsequent formation of large drug aggregates, covalently linked drug dimers were designed[5a] Based on the co-precipitation of the dimeric drug and a di-block copolymer, nanoparticles with drug core and a polymer shell were produced with more than 50% drug loading. A superfast sequential microfluidic nanoprecipitation was developed for preparing drug-core polymer-shell nanocomposites with a 45% drug loading.[5b] These two approaches provide new strategies for forming drug-core polymeric shell nanoparticles with high drug loading. However, developing a versatile and controllable drug encapsulation system with high drug loading is a challenge, and the effect of drug loading on in vivo anti-cancer efficacy remains unexplored.

Here, we adopted a biomolecule templating strategy to create various drug-core silica-shell nanoparticles with exceptionally high drug loadings of up to 65% and encapsulation efficiency of more than 99%. High drug loading nanoparticles demonstrated more efficient cellular uptake compared to low drug loading nanoparticles, leading to improved anti-cancer action and reduced side effects. This straightforward bioinspired approach for producing core-shell nanoparticles with high drug loading offers a new strategy to improve the delivery of hydrophobic therapeutic drugs.

Results and Discussion

Design and characterization of high drug loading nanoparticles (NPs)

Our strategy is to form stable drug NPs as the core in the presence of a dual-functional peptide SurSi through nanoprecipitation, followed by biosilicification at the drug surface thus forming a silica shell (Figure 1A). The SurSi peptide (Ac-MKQLAHSVSRLEHA RKKRKKRKKRKKGGGY-CONH$_2$) was designed to have two modules,[6] namely, the Sur module (MKQLAHS VSRLEHA) with two heptad repeats for surface activity (blue and yellow helix in Figure 1A),[7] and the Si module with a dense pack of positively-charged amino acids (RKK RKKRKKRKKGGGY-CONH$_2$) for biosilicification (green tail) at room temperature, neutral pH and without the requirement of any toxic chemicals.

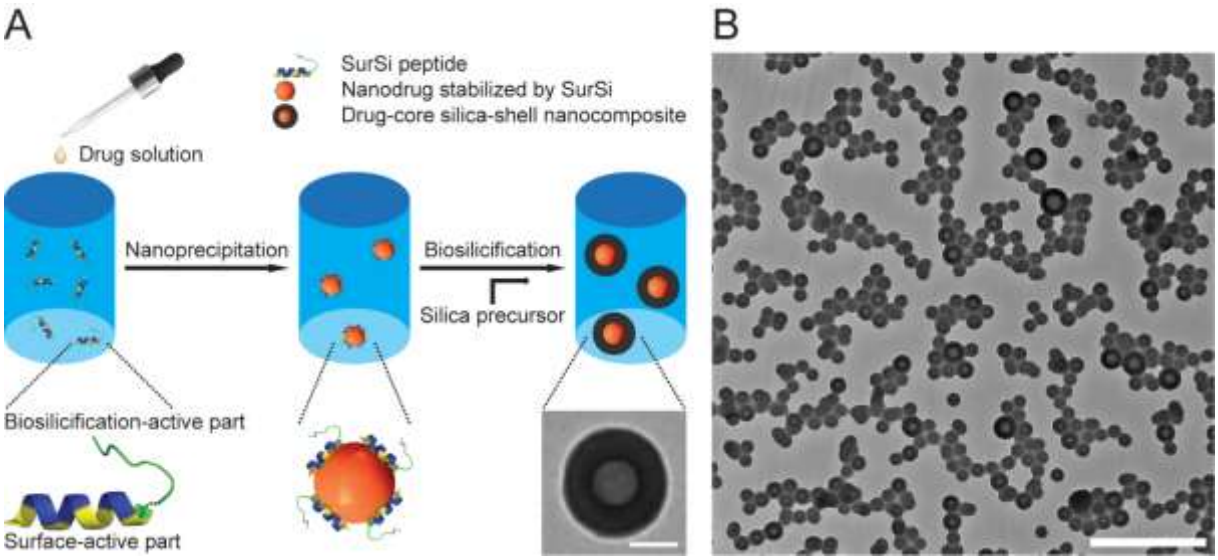

Figure 1. Design of drug-core silica-shell nanocomposites using a bi-functional peptide. (**A**) Schematic illustration of the synthesis process of drug-core silica-shell nanocomposites. Scale bar, 50 nm. Drug NPs were formed through nanoprecipitation and stabilized by a bi-

functional peptide which could later induce the formation of a silica shell around the drug NP, creating the drug-core silica-shell nanocomposite. (**B**) Representative transmission electron microscopy (TEM) image of curcumin-core silica-shell nanocomposites. Scale bar, 1 μm.

Firstly, curcumin, as a model hydrophobic drug, was dissolved in an organic solvent (such as acetone, ethanol, and dimethyl sulfoxide). The solvent containing curcumin was then added to the SurSi solution (in HEPES buffer, pH 7.5) dropwise with stirring. Curcumin NPs were formed through a nanoprecipitation process. The curcumin NPs were stabilized by SurSi because of its surfactant functionality and the electrical repulsion (zeta potential of SurSi stabilized curcumin NP > +30 mV, Table S1). Then a silica precursor, triethoxyvinylsilane, was added to the curcumin NP suspension to initiate biosilicification at the drug surface under room temperature and gentle stirring. After 48 h reaction, uniform and well dispersed drug-core silica-shell nanocomposites were observed with a clear core-shell structure (Figure 1B), and 5.3% drug loading was achieved because of the thick silica shell. However, when we applied this approach to a more hydrophobic anticancer drug, paclitaxel, drug aggregates instead of uniform nanodrugs formed because SurSi has an insufficient surface activity to stabilize the paclitaxel NPs (Table S1).

To stabilize paclitaxel NPs, we next designed a new modular peptide CAMSi ($CH_3(CH_2)_7CO$-MKQLADSLHQLARQVSRLEHA RKKRKKRKKRKKGGGY-$CONH_2$) consisting of three modules (Figure 2A), i.e., a new surface-active module (MKQLADS LHQLARQVSRLEHA, blue and yellow helix), the Si module (RKKRKKRKKRKKGGGY-$CONH_2$, green tail), and a hydrophobic tail module ($CH_3(CH_2)_7CO$-, orange section). Compared to the dual-modular SurSi, the CAMSi has a longer surface-active module with three heptad repeats (MKQLADS LHQLARQ VSRLEHA) to augment the surface activity. To further enhance the interaction between the peptide and the hydrophobic drug core, a nonanoic acid moiety ($CH_3(CH_2)_7CO$-) was added to the N-terminus. The aliphatic chain acts as a hydrophobic "anchor" attaching to the hydrophobic phase, thus allowing strong hydrophobic interactions between CAMSi and the hydrophobic drug. We have previously demonstrated the enhanced surface activity induced by adding the nonanoic acid moiety to peptide surfactants.[8] It is expected that a longer carbon chain (C_{10} or even longer C_{16}) will give even stronger anchoring effect, but will also reduce the solubility of CAMSi as well as change the adsorption kinetics. The longer the carbon chain, the lower the solubility and the slower adsorption to the interface would be. Considering this dilemma, we selected C_8 as the hydrophobic anchor. As expected, CAMSi demonstrated an enhanced surface activity compared to SurSi as evidenced by the results of drop shape analysis (Figure S1). In a similar method described above, solvents containing paclitaxel were added to the CAMSi buffer solution. Paclitaxel NPs with uniform size were formed in the presence of CAMSi, in contrast to micron-size paclitaxel rods and large aggregates in the absence of CAMSi (Figure S2). Also, CAMSi can stabilize other hydrophobic NPs such as curcumin and fluorescent dye (DiI) NPs (Figure S2), demonstrating its versatility in NP stabilization. In the absence of CAMSi, these hydrophobic molecules (paclitaxel, curcumin, and DiI) tend to rapidly precipitate and form large aggregates (Figure 2F,I,L). Furthermore, the size of the drug NPs can be tuned by simply changing the CAMSi concentration (Table S2). The paclitaxel NPs stabilized by CAMSi can be stable for up to 24 h (Figure S3). To achieve long-term stability, paclitaxel-core silica-shell nanocomposites were formed upon the addition of a silica precursor (triethoxyvinylsilane) due to the biosilicification activity of the Si module in the CAMSi. Energy dispersive X-ray and Fourier-transform infrared spectroscopy analysis confirmed the successful growth of a silica shell (Figures S4 and S5). Other cargo-core silica-shell nanocomposites (curcumin and DiI) can be synthesized using the same approach. These cargo-core silica-shell nanocomposites remained stable and well dispersed for more than a month as

10.1002/anie.201908357

homogeneous and semi-transparent suspensions (Figure 2H,K,N and Figure S6). Furthermore, CAMSi generated a much thinner silica layer compared to the thick shell structure formed by SurSi (Figures 1B and 2C), as observed from TEM images and also from the small particle size change using dynamic light scattering (Figure S2 and Table S3). The synthesized drug-core silica-shell nanocomposites exhibit positive charges (~ +30 mV), which can be easily modified to have different surface properties (PEGylation, conjugation with targeting ligands, etc.).[9]

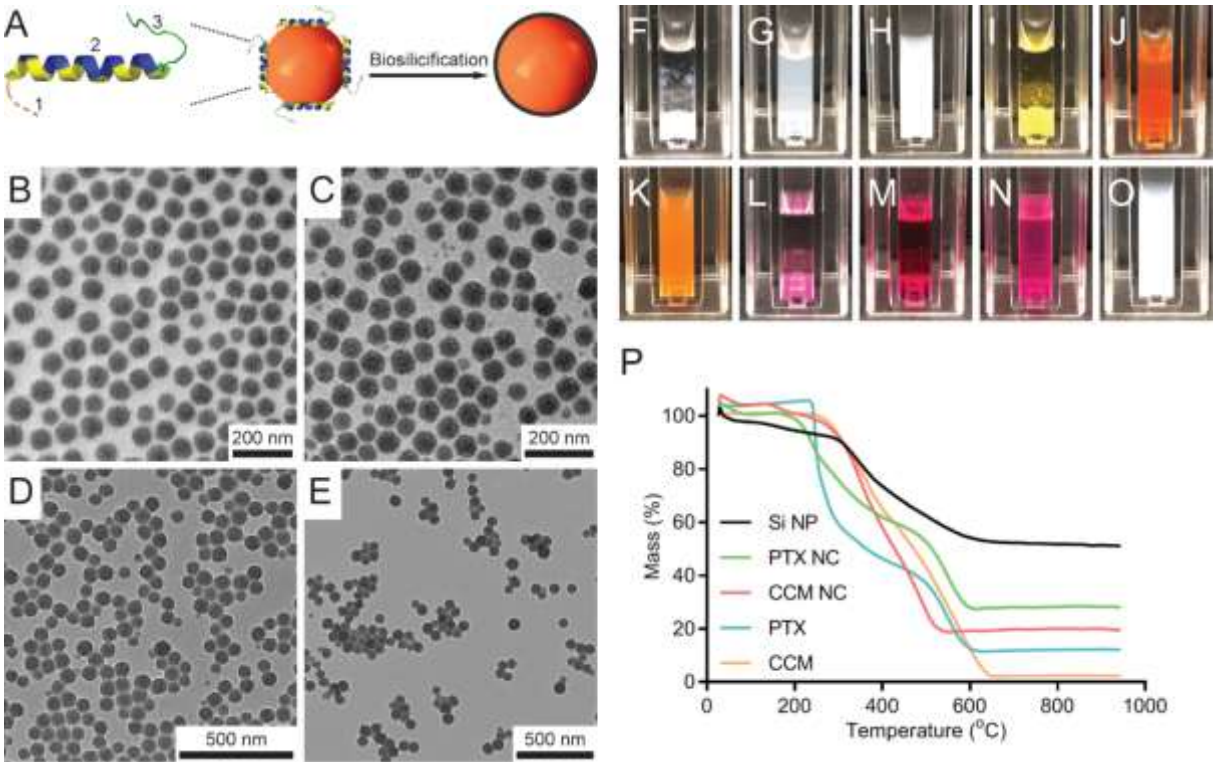

Figure 2. Formation of drug-core thin-silica-shell nanocomposites with high drug loading. (**A**) Schematic demonstration showing the formation of drug-core thin-silica-shell nanocomposites using the tri-modular peptide CAMSi consisting of (**1**) Nonanoic acid, (**2**) Surface-active, and (**3**) Biosilicification-active parts. Representative TEM images of (**B**) Paclitaxel-core silica-shell nanocomposites, (**C**) Curcumin-core silica-shell nanocomposites, (**D**) DiI-core silica-shell nanocomposites, and (**E**) Plain silica NPs. Photographs of suspensions of (**F**) Paclitaxel precipitates from nanoprecipitation in the absence of CAMSi, (**G**) Paclitaxel NPs stabilized by CAMSi, (**H**) Paclitaxel-core silica-shell nanocomposites, (**I**) Curcumin precipitates formed by nanoprecipitation in the absence of CAMSi, (**J**) Curcumin NPs stabilized by CAMSi, (**K**) Curcumin-core silica-shell nanocomposites, (**L**) DiI precipitates from nanoprecipitation in the absence of CAMSi, (**M**) DiI NPs stabilized by CAMSi, (**N**) DiI-core silica-shell nanocomposites, and (**O**) silica NPs induced from CAMSi. (**P**) Thermogravimetric analysis profiles of silica NPs induced by CAMSi (Si NP), paclitaxel-core silica-shell nanocomposites (PTX NC), curcumin-core silica-shell nanocomposites (CCM NC), paclitaxel (PTX), and curcumin (CCM). The drug loadings were calculated from the weight loss during heating.

To assess the drug loading efficiency of these drug-core silica-shell nanocomposites, thermogravimetric analysis was carried out (Figure 2P). Maximum drug loadings of 59.2% and 64.9% were achieved for paclitaxel and curcumin, respectively. Furthermore, we can adjust drug loadings by tuning the drug-core sizes (Table S2). For example, for drug cores of 31.6 nm and silica shell thickness of 4.7 nm, the drug loading was 29.3%. When the drug core was increased to 60.3 and 83.9 nm, the drug loadings were 51.2% and 65.3%, respectively. The

10.1002/anie.201908357

encapsulation efficiencies for paclitaxel nanocomposites, curcumin nanocomposites, and DiI nanocomposites were 99.3%, 99.9%, and 99.5%, respectively (Table S4). Furthermore, the amorphous drug structure was confirmed by the disappeared characteristic melting peaks of paclitaxel and curcumin (Figure S7), as well as the continuous diffraction rings in the electron diffraction pattern (Figure S8). This amorphous property is beneficial for drug NPs as their solubility can be greatly enhanced.[10]

In vitro cellular uptake of high drug loading (HDL) and low drug loading (LDL) NPs

One of the most important advantages of HDL NPs is that a sufficient therapeutic level can be achieved by using the least number of NPs. In other words, if 1,000 NPs are required to reach a certain therapeutic concentration with a drug loading of 50%, then 5,000 NPs with a drug loading of 10% are needed to achieve the same drug concentration in cells. This is very challenging as cells may only take up a limited number of NPs. We investigated the cellular uptake capacity of a model cancer cell SKOV3 using plain silica NPs, which had no drug core but the same material as the shell of the drug-core silica-shell nanocomposites. These silica NPs were synthesized by directly hydrolyzing triethoxyvinylsilane in the presence of CAMSi, and they had the same diameter of ~70 nm as the drug-core silica-shell nanocomposites (Table S3). The silica NPs of different particle concentrations (determined by a Nanosight particle tracker) were incubated with SKOV3 cancer cells. After 4 h incubation, the medium solution containing NPs were removed and characterized by the Nanosight to determine the residual particle concentration. The difference between the initial and final particle concentration was calculated as the particle uptake by SKOV3. We found that particle uptake per cell gradually increased with an increase of the administrated silica NP concentrations, and peaked at an administrated NP concentration of 6.3×10^5 NP cell^{-1} (Figure 3A), then decreased slightly and remained constant with further increasing NP concentration to 1.0×10^7 NP cell^{-1}. A maximum of 1.9×10^5 particles could be taken up by a single SKOV3 cell, demonstrating its uptake limit under such conditions. We also calculated the percentage of NPs being taken up during incubation (Figure 3A). A constant decrease was observed with an increase of administrated NP concentrations. For example, when the particle concentration was low (1.5×10^2 NP cell^{-1}), near 100% of the particles were taken up. However, when it was increased to 1×10^5 NP cell^{-1}, the cells can only take up about 40% of the NPs. Therefore, we hypothesize that less NPs with HDL will give higher uptake efficiency, thus better drug efficacy.

10.1002/anie.201908357

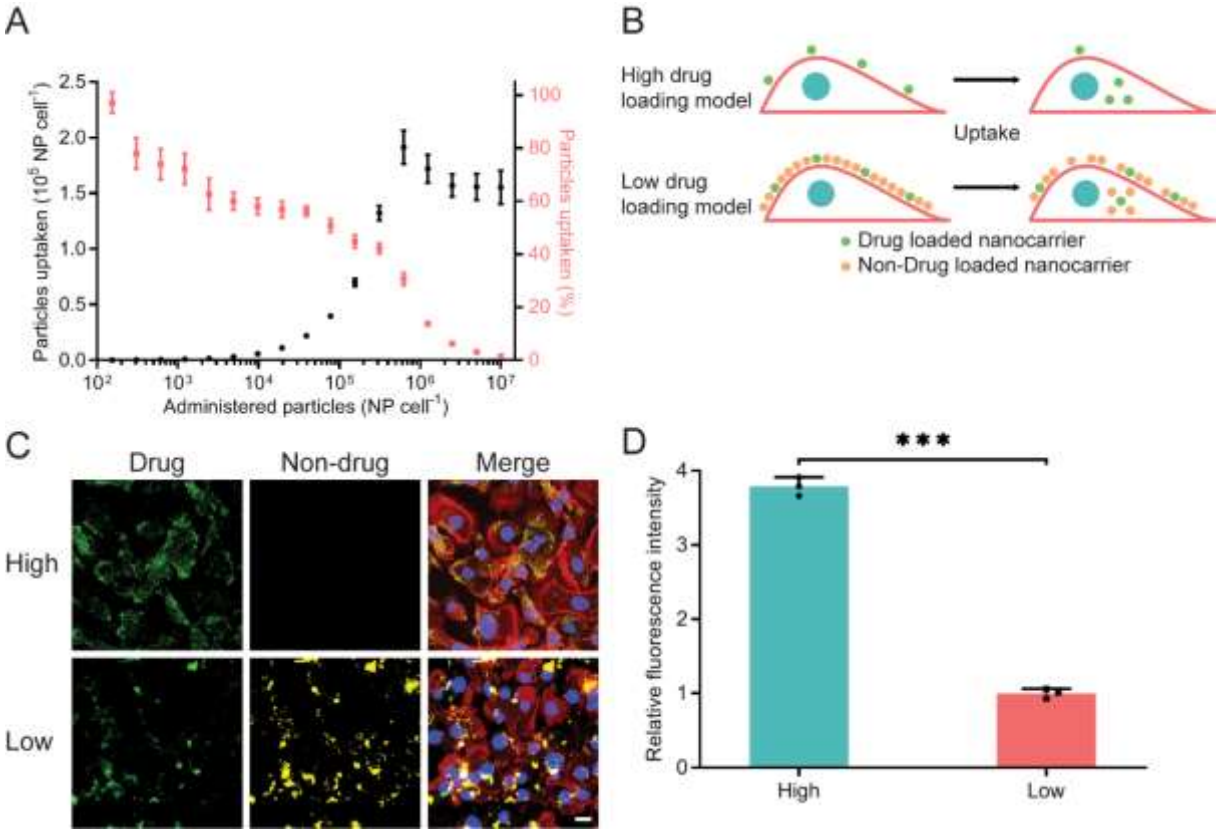

Figure 3. Cellular uptake of different NPs. (**A**) Uptake of silica NPs by SKOV3 cells. Both the absolute amount (black, left y-axis) and percentage (red, right y-axis) of cellular uptake of particles are illustrated. The mean ± s.d. from three independent replicates is shown. (**B**) Schematic illustration of cellular uptake of HDL and LDL NPs. (**C**) Representative CLSM images of SKOV3 cellular uptake of HDL and LDL NPs. Scale bar, 20 μm. The HDL model consists of curcumin-core silica-shell nanocomposites (green, as drug), whereas the LDL model consists of a mixture of curcumin-core and DiI-core (yellow, as non-drug) silica-shell nanocomposites. The HDL and LDL models had the same concentration of curcumin. Same CLSM settings were used. (**D**) Quantitative cellular uptake of HDL and LDL NPs by flow cytometry. The HDL model consisted of curcumin (as drug) nanocomposites at a concentration of 1.0×10^6 NP cell^{-1}, and the LDL model consisted of a mixture of curcumin nanocomposites (the same concentration as the HDL model) and silica NPs (four times particle concentration of the curcumin nanocomposites). Due to the limit of cellular uptake, the drug uptake demonstrated a huge difference. The mean ± s.d. from three independent replicates is shown. ***$P < 0.001$, analyzed by two-tailed Student's *t*-test.

To test our hypothesis, we established an assay to quantify the uptake of HDL and LDL NPs (Figure 3B). Specifically, we selected the drug-core silica-shell nanocomposites with 50% drug loading as the HDL model. To simulate the LDL of 10%, we mixed the drug-core silica-shell nanocomposites having 50% drug loading with four times of plain silica NPs (non-drug NPs). The plain silica NPs or non-drug NPs were fabricated to have the same size, shape, surface material and surface charge as that of the drug-loaded nanocomposites, so they should have the same opportunity to be taken up by cancer cells. The two systems have the same amount of drugs, but the LDL system had four times more NPs than the HDL system.

The HDL and LDL models were used to carry out cellular uptake experiments qualitatively using confocal laser scanning microscope (CLSM) and quantitatively using flow cytometry. In the qualitative study (Figure 3C and Figure S9), we used the curcumin-core silica-shell

nanocomposites (curcumin nanocomposites) with 50% drug loading at an NP concentration of 1.0×10^6 NP cell^{-1} as the HDL model as curcumin itself has fluorescence. The LDL model was a mixture of curcumin nanocomposites at an NP concentration of 1.0×10^6 NP cell^{-1} and DiI-core silica-shell nanocomposites (DiI as the non-drug) at an NP concentration of 4.0×10^6 NP cell^{-1}. Both nanocomposites had similar sizes and surface charges (Table S3). After incubating for 4 h, the SKOV3 cells demonstrated a significantly higher drug uptake efficiency (green color) in the HDL model than the LDL model, mainly due to the competitive uptake of the non-drug NPs in the LDL model (DiI-core silica-shell nanocomposites, yellow color, Figure 3C). Similarly, the flow cytometry result demonstrated significantly stronger fluorescence intensity (around four-fold higher) of the HDL model than that of the LDL model (Figure 3D and Figure S10). To avoid interference of fluorescence signals in the flow cytometry experiment for the LDL model, we used plain silica NPs to mix with the HDL nanocomposites instead of the DiI-core silica-shell NPs. The significant difference in fluorescence intensity between the HDL and LDL models was purely due to the limit of NP uptake by the SKOV3 cells, which validated our hypothesis that exposure to fewer NPs with higher drug loading results in higher uptake efficiency.

In vitro cytotoxicity of HDL and LDL NPs

The difference in cellular uptake between the HDL and LDL models led us to speculate that this would have an impact on their cell cytotoxicity. We prepared different drug-core silica-shell NPs (paclitaxel and curcumin) with HDL and LDL (50% and 10% drug loadings) (Figure 4 and Figures S11). For the paclitaxel nanocomposites, the particle concentrations of HDL and LDL models were selected as 6.2×10^4 NP cell^{-1} and 3.1×10^5 NP cell^{-1} (where both drug concentrations were 1 μM, 0.9 μg mL^{-1}). For the curcumin nanocomposites, the particle concentrations of HDL and LDL models were selected as 9.3×10^5 NP cell^{-1} and 4.7×10^6 NP cell^{-1} (where both drug concentrations were 40 μM, 14.7 μg mL^{-1}). We incubated these drug-loaded NPs with SKOV3 cancer cells for 48 h (Figure 4). The plain silica NPs (4.7×10^6 NP cell^{-1}) showed low cytotoxicity (<20% mortality), whereas all drug-core silica-shell nanocomposites demonstrated high cytotoxicity. It is also clear that both (paclitaxel and curcumin) HDL models showed significantly higher cytotoxicity than the corresponding LDL models, which agrees well with the cellular uptake results. At the same time, we noticed that the difference between the two curcumin groups was dramatic in comparison with the paclitaxel groups, mainly due to the much higher half maximal inhibitory concentration (IC_{50}) of curcumin (4.8 μg mL^{-1}) than for paclitaxel (0.04 μg mL^{-1}) (Figure S12). The significantly higher cytotoxicity of HDL NPs demonstrated their unique advantages over LDL NPs. The drug release study of the curcumin nanocomposites showed an accelerated release of the drug at pH 4.5, but minimum release at pH 7.4 due to the faster degradation of the silica shell in acidic solutions (Figures S13 and S14).[11]

10.1002/anie.201908357

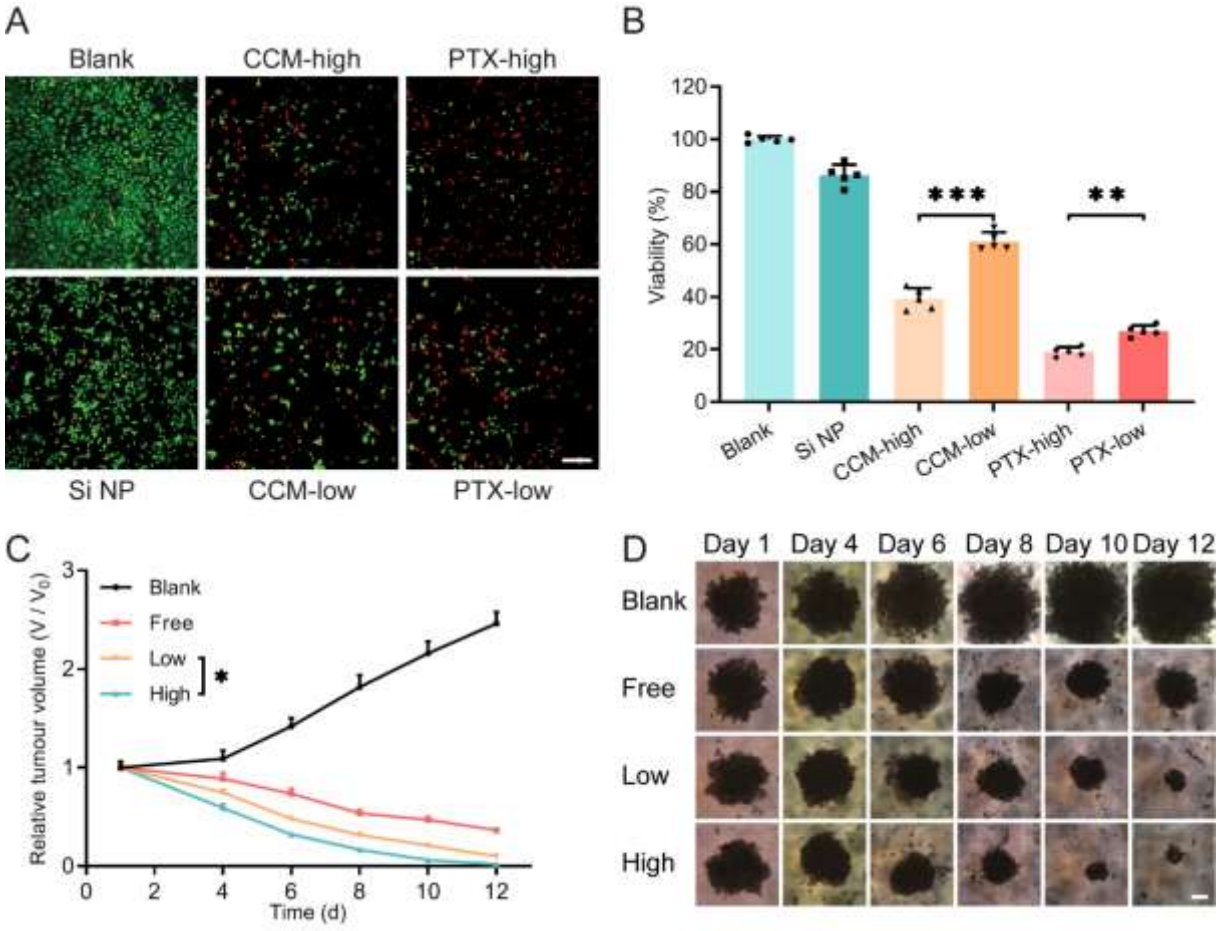

Figure 4. In vitro cytotoxicity of HDL and LDL NPs using SKOV3 cells. (**A**) Representative CLSM images of SKOV3 cells stained by the live/dead cell double staining kit after incubating for 48 h with silica NPs (Si NP), curcumin (CCM) nanocomposites, and paclitaxel (PTX) nanocomposites with HDLs and LDLs (different particle concentrations but same amount of drugs). The green and red colors represent live and dead cells, respectively. Scale bar, 100 μm. (**B**) Viability of SKOV3 cells after incubating with silica NPs, curcumin nanocomposites, and paclitaxel nanocomposites with HDLs and LDLs for 48 h (determined by cell proliferation reagent WST-1). The mean ± s.d. from five independent replicates is shown. ***$P < 0.001$, **$P < 0.01$, analyzed by one-way analysis of variance (ANOVA). (**C**) Growth curve of SKOV3 tumor spheroids treated with free paclitaxel, high and low paclitaxel-loading silica nanocomposites during a course of 12 days. Free paclitaxel was produced by nanoprecipitation of paclitaxel-DMSO solution in cell culture medium. All drug-treated groups contained 100 ng mL^{-1} paclitaxel. The mean ± s.d. from five independent replicates is shown. *$P < 0.05$, analyzed by one-way ANOVA. (**D**) Representative photographs of tumor spheroids in (**C**). Scale bar, 100 μm.

Next, we performed the cytotoxicity test on the 3D SKOV3 tumor spheroids using HDL and LDL silica nanocomposites containing 100 ng mL^{-1} paclitaxel.[12] As we expected, after the treatment, the HDL group showed smaller spheroid volume and lower viability among all the treated groups (Figure 4C,D and Figure S15), demonstrating its enhanced tumor inhibition effect.

In vivo anti-tumor effects of HDL and LDL NPs

10.1002/anie.201908357

In vivo anti-tumor studies were carried out using a murine xenograft model. Four groups including PBS, free paclitaxel, HDL NPs (PEGylated paclitaxel nanocomposites, 41% drug loading), and LDL NPs (the mixture of PEGylated paclitaxel nanocomposites and four times PEGylated plain silica NPs, 8% drug loading) were injected intravenously at three days intervals for a total of five injections, at an equivalent dose of 0.1 mg paclitaxel per mouse each time. Free paclitaxel was prepared by dissolving it in DMSO followed by adding into PBS containing 1% polysorbate 80. During the treatment, the HDL group had the highest body weight (Figure 5A). It also demonstrated better anti-tumor efficacy compared to the free drug and LDL groups within 25 days showing significantly smaller tumor volume and weight (Figure 5B-D). To achieve the same drug concentration, the administered LDL NPs (6.37×10^{11} NPs in 100 μL) was five times concentrated than the HDL NPs (Figure 5E,F), so the LDL sample was much more viscous which makes it difficult and risky for intravenous injection. Also, over-dosed nanomaterials may cause toxic effects.[13] Hematoxylin and eosin (H&E) staining of tumors revealed advanced tumor necrosis in the HDL group (Figure 5G), but much less necrosis in the LDL group, demonstrating the stronger anti-tumor effect of the HDL NPs.[14] Though the HDL group showed greater inhibition of tumor growth, it appeared less toxicity on all major organs, as no obvious pathological change in the HDL group could be observed compared to that in the PBS group. However, the LDL group demonstrated significant lesions in the liver and kidney, probably due to the toxicity of the excess materials. Further analysis of organ-body weights confirmed the better safety of HDL NPs compared to the low counterparts (Figure S16). Together, these results indicate that the HDL nanomedicine demonstrates 1) enhanced anti-tumor efficacy even when the drug concentrations are the same, 2) easier administration because of the smaller number of NPs and lower viscosity of the solution, and 3) reduced toxicity and side effects in contrast to the LDL nanomedicine. Notably, the concentration of anti-cancer drug paclitaxel used in this study was 5 mg kg^{-1} mice, so 2.4 and 12.2 g L^{-1} NPs with HDL and LDL, respectively, were in the intravenous injection liquid. This dose has the potential to be increased ten folds to 50 mg kg^{-1} mice for the HDL formulation (41% loading, 24 g L^{-1} NPs in the intravenous injection liquid), but would be impossible for the LDL formulation with 8% loading, because 122 g L^{-1} NPs would be required for intravenous injection which is too concentrated. Therefore, the HDL strategy offers broad opportunities for hydrophobic chemotherapeutic drug delivery.

10.1002/anie.201908357

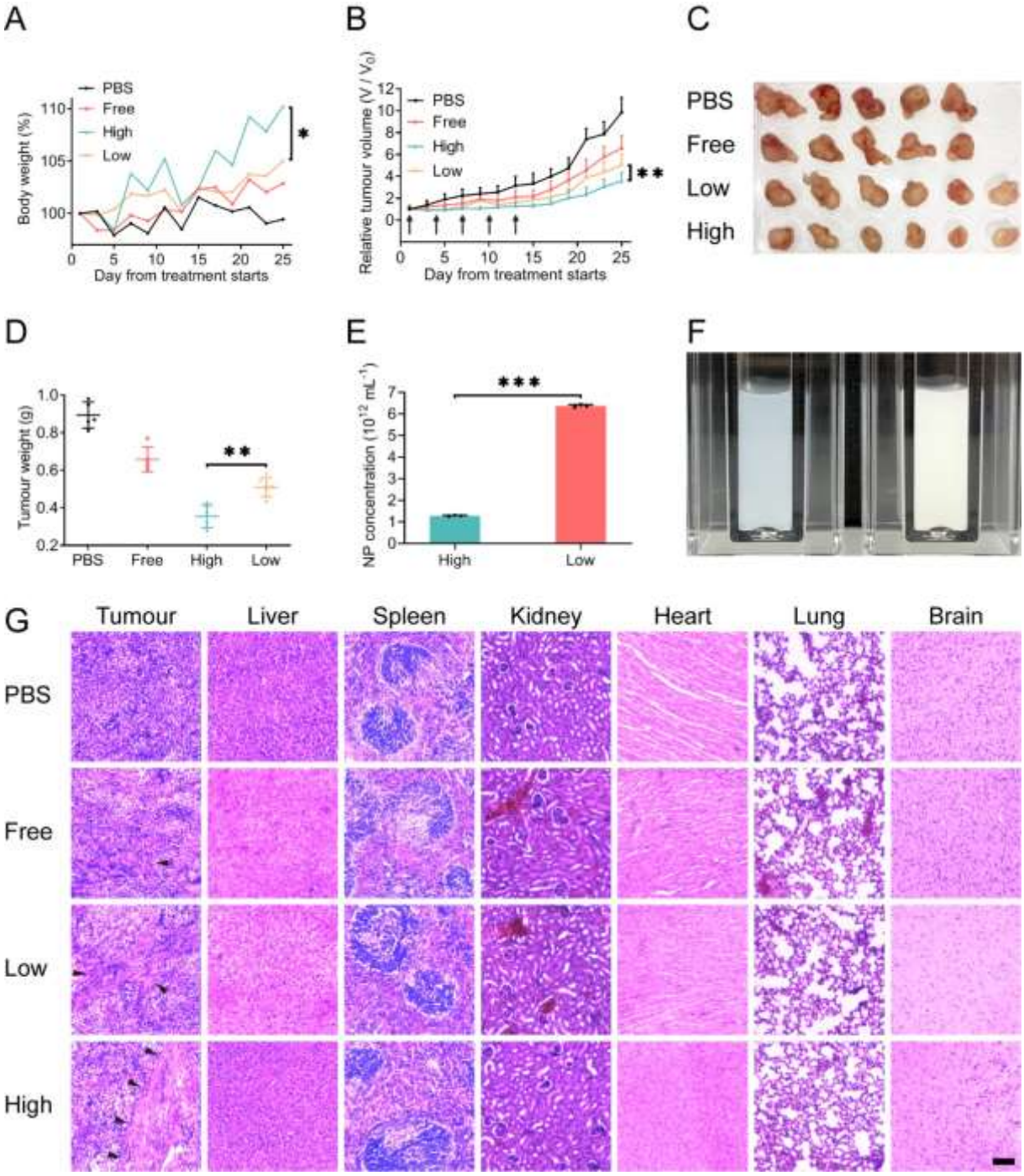

Figure 5. In vivo anti-tumor effects of HDL and LDL silica nanocomposites. (A) The body weights and (B) Tumor volumes of the mice measured every 2 days. Drug injection days are indicated with black arrows. Data are reported as mean (A) and mean ± s.d. (B) (n = 5 or 6). *P < 0.05, **P < 0.01, analyzed by one-way ANOVA. (C) Photographs and (D) Tumor weights of harvested tumors on the day 25. Data are reported as mean ± s.d. (n = 5 or 6). **P < 0.01, analyzed by one-way ANOVA. (E) NP concentrations of HDL and LDL silica nanocomposites used for the experiment were determined by a Nanosight particle tracker. The mean ± s.d. from three independent replicates is shown. ***P < 0.001, analyzed by two-tailed Student's *t*-test. (F) Photograph of high (left) and low (right) drug loading silica nanocomposites used for the in vivo experiment. (G) Tumors and major organs harvested on day 25 were stained with hematoxylin and eosin (H&E). Necrotic tissues are indicated by black arrows. Scale bar, 100 μm. Data are representative of the same group.

Conclusion

This study reports the synthesis of drug-core silica-shell nanocomposites with exceptionally high drug loadings (up to 65%) and encapsulation efficiencies (>99%). This platform technology is based on a modular design of dual-functional peptides, which have excellent surface activity and biosilicification activity. By tuning the size of the drug core, nanoparticles with tunable drug loadings can be achieved. This technology has the potential for encapsulating various hydrophobic molecules. This work also developed high and low drug loading models to fundamentally explore the effect of drug loading on cellular uptake and cell cytotoxicity. We showed that high drug loading nanoparticles exhibited more efficient cellular uptake and enhanced cytotoxicity than those low drug loading nanoparticles in vitro, mainly due to the limited cellular uptake. Furthermore, the high drug loading nanoparticles demonstrated improved anti-tumor efficacy but lower side effects in vivo. Therefore, it is vital to develop nanoparticles with high drug loading to achieve effective therapeutic levels. The biomolecular templating technology described here offers a strategy for the manufacture of drug-core nanocomposite with high drug loading, and opens unique opportunities for drug encapsulation and drug delivery applications.

Acknowledgements

This work was supported by the Australian Research Council (DP150100798, FT140100726, and CE140100036). This research was supported by Australian Government Research Training Program Scholarships. The authors acknowledge Dr Robert Sullivan for the help on histology study. The authors acknowledge Barb Arnts and David Herne for the animal work service. The authors acknowledge the facilities, and the scientific and technical assistance, of the Australian Microscopy & Microanalysis Research Facility at the Centre for Microscopy and Microanalysis, The University of Queensland. This work was performed in part at the Queensland node of the Australian National Fabrication Facility, a company established under the National Collaborative Research Infrastructure Strategy to provide nano and microfabrication facilities for Australia's researchers.

Conflict of interest

The authors declare the following competing interests: The University of Queensland (UQ) filed a patent on the use of mineralizing peptides for making silica nanocapsules. D.W., A.P.J.M. and C.-X.Z. are named inventors on this patent and through their employment with UQ hold an indirect interest in this intellectual property. The other authors declare no competing interest.

Keywords: Nanoparticles • Drug delivery • Peptides • Cancer • Biomimetic synthesis

[1] a) R. P. Lyon, T. D. Bovee, S. O. Doronina, P. J. Burke, J. H. Hunter, H. D. Neff-LaFord, M. Jonas, M. E. Anderson, J. R. Setter, P. D. Senter, *Nat. Biotechnol.* **2015**, *33*, 733; b) A. N. Zelikin, C. Ehrhardt, A. M. Healy, *Nat. Chem.* **2016**, *8*, 997; c) B. E. Rabinow, *Nat. Rev. Drug Discovery* **2004**, *3*, 785; d) K. M. Wasan, D. R. Brocks, S. D. Lee, K. Sachs-Barrable, S. J. Thornton, *Nat. Rev. Drug Discovery* **2008**, *7*, 84; e) J. R. Junutula, H. Raab, S. Clark, S. Bhakta, D. D. Leipold, S. Weir, Y. Chen, M. Simpson, S. P. Tsai, M. S. Dennis, *Nat. Biotechnol.* **2008**, *26*, 925; f) L. Gao, G. Liu, J. Ma, X.

Wang, L. Zhou, X. Li, F. Wang, *Pharm. Res.* **2013**, *30*, 307-324; g) Y. Cai, H. Shen, J. Zhan, M. Lin, L. Dai, C. Ren, Y. Shi, J. Liu, J. Gao, Z. Yang, *J. Am. Chem. Soc.* **2017**, *139*, 2876-2879.

[2] a) S. Kalepu, V. Nekkanti, *Acta Pharm. Sin. B* **2015**, *5*, 442-453; b) P. Couvreur, *Adv. Drug Delivery Rev.* **2013**, *65*, 21-23.

[3] a) B. Duncan, C. Kim, V. M. Rotello, *J. Controlled Release* **2010**, *148*, 122-127; b) J. Hrkach, D. Von Hoff, M. M. Ali, E. Andrianova, J. Auer, T. Campbell, D. De Witt, M. Figa, M. Figueiredo, A. Horhota, *Sci. Transl. Med.* **2012**, *4*, 128ra139-128ra139; c) Y. Lu, Z. Yue, J. Xie, W. Wang, H. Zhu, E. Zhang, Z. Cao, *Nat. Biomed. Eng.* **2018**, *2*, 318; d) R. Kanasty, J. R. Dorkin, A. Vegas, D. Anderson, *Nat. Mater.* **2013**, *12*, 967; e) G. Mikhaylov, U. Mikac, A. A. Magaeva, V. I. Itin, E. P. Naiden, I. Psakhye, L. Babes, T. Reinheckel, C. Peters, R. Zeiser, *Nat. Nanotechnol.* **2011**, *6*, 594; f) V. P. Torchilin, *Nat. Rev. Drug Discovery* **2014**, *13*, 813; g) P. Horcajada, T. Chalati, C. Serre, B. Gillet, C. Sebrie, T. Baati, J. F. Eubank, D. Heurtaux, P. Clayette, C. Kreuz, *Nat. Mater.* **2010**, *9*, 172; h) L. Y. Chou, K. Zagorovsky, W. C. Chan, *Nat. Nanotechnol.* **2014**, *9*, 148; i) E. P. Thi, C. E. Mire, A. C. Lee, J. B. Geisbert, J. Z. Zhou, K. N. Agans, N. M. Snead, D. J. Deer, T. R. Barnard, K. A. Fenton, *Nature* **2015**, *521*, 362; j) J. Bhattacharyya, J. J. Bellucci, I. Weitzhandler, J. R. McDaniel, I. Spasojevic, X. Li, C.-C. Lin, J.-T. A. Chi, A. Chilkoti, *Nat. Commun.* **2015**, *6*, 7939.

[4] a) Z. Liu, Y. Jiao, Y. Wang, C. Zhou, Z. Zhang, *Adv. Drug Delivery Rev.* **2008**, *60*, 1650-1662; b) G. A. Husseini, W. G. Pitt, *Adv. Drug Delivery Rev.* **2008**, *60*, 1137-1152; c) L. Zhang, J. M. Chan, F. X. Gu, J.-W. Rhee, A. Z. Wang, A. F. Radovic-Moreno, F. Alexis, R. Langer, O. C. Farokhzad, *ACS Nano* **2008**, *2*, 1696-1702; d) Y. Matsumura, *Adv. Drug Delivery Rev.* **2008**, *60*, 899-914; e) K.-J. Chen, L. Tang, M. A. Garcia, H. Wang, H. Lu, W.-Y. Lin, S. Hou, Q. Yin, C. K.-F. Shen, J. Cheng, *Biomaterials* **2012**, *33*, 1162-1169; f) J. Cheng, B. A. Teply, I. Sherifi, J. Sung, G. Luther, F. X. Gu, E. Levy-Nissenbaum, A. F. Radovic-Moreno, R. Langer, O. C. Farokhzad, *Biomaterials* **2007**, *28*, 869-876.

[5] a) K. Cai, X. He, Z. Song, Q. Yin, Y. Zhang, F. M. Uckun, C. Jiang, J. Cheng, *J. Am. Chem. Soc.* **2015**, *137*, 3458-3461; b) D. Liu, H. Zhang, S. Cito, J. Fan, E. Mäkilä, J. Salonen, J. Hirvonen, T. M. Sikanen, D. A. Weitz, H. l. A. Santos, *Nano Lett.* **2017**, *17*, 606-614; c) S. Lv, Y. Wu, K. Cai, H. He, Y. Li, M. Lan, X. Chen, J. Cheng, L. Yin, *J. Am. Chem. Soc.* **2018**.

[6] D. Wibowo, C.-X. Zhao, A. P. Middelberg, *Chem. Commun.* **2014**, *50*, 11325-11328.

[7] A. F. Dexter, A. S. Malcolm, A. P. Middelberg, *Nat. Mater.* **2006**, *5*, 502.

[8] H.-F. Wang, D. Wibowo, Z. Shao, A. P. Middelberg, C.-X. Zhao, *Langmuir* **2017**, *33*, 7957-7967.

[9] Y. Hui, D. Wibowo, Y. Liu, R. Ran, H.-F. Wang, A. Seth, A. P. Middelberg, C.-X. Zhao, *ACS Nano* **2018**, *12*, 2846-2857.

[10] E. Amstad, M. Gopinadhan, C. Holtze, C. O. Osuji, M. P. Brenner, F. Spaepen, D. A. Weitz, *Science* **2015**, *349*, 956-960.

[11] G.-Z. Yang, D. Wibowo, J.-H. Yun, L. Wang, A. P. Middelberg, C.-X. Zhao, *Langmuir* **2017**, *33*, 5777-5785.

[12] J. Friedrich, C. Seidel, R. Ebner, L. A. Kunz-Schughart, *Nat. Protoc.* **2009**, *4*, 309.

[13] a) A. Nel, T. Xia, L. Mädler, N. Li, *Science* **2006**, *311*, 622-627; b) F. Peng, M. I. Setyawati, J. K. Tee, X. Ding, J. Wang, M. E. Nga, H. K. Ho, D. T. Leong, *Nat. Nanotechnol.* **2019**, *14*, 279.

[14] a) S. Li, Q. Jiang, S. Liu, Y. Zhang, Y. Tian, C. Song, J. Wang, Y. Zou, G. J. Anderson, J.-Y. Han, *Nat. Biotechnol.* **2018**, *36*, 258; b) D. Chen, B. Li, S. Cai, P. Wang, S. Peng, Y. Sheng, Y. He, Y. Gu, H. Chen, *Biomaterials* **2016**, *100*, 1-16.

10.1002/anie.201908357

Entry for the Table of Contents

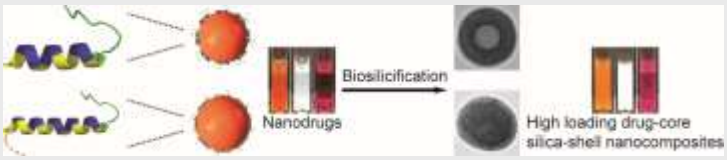

Difunctional amphiphilic peptides were designed to not only stabilize hydrophobic drug nanoparticles but also induce biosilicification at the drug particle surface to maintain the long-term stability of the nano-drug. For the first time we report the fabrication of drug-core silica-shell nanocomposites having exceptionally high drug loading (up to 65% w/w) and encapsulation efficiencies (>99%).

*Guangze Yang, Yun Liu, Haofei Wang, Russell Wilson, Yue Hui, Lei Yu, David Wibowo, Cheng Zhang, Andrew K. Whittaker, Anton P. J. Middelberg, and Chun-Xia Zhao**

Page No. – Page No.

Bioinspired Core-Shell Nanoparticles for Hydrophobic Drug Delivery